Signal Processing 93 (2013) 2942–2955

Contents lists available at SciVerse ScienceDirect

Signal Processing

journal homepage: www.elsevier.com/locate/sigpro

Oversampled perfect reconstruction DFT modulated filter banks for multi-carrier transceiver systems ☆

Siavash Rahimi *, Benoit Champagne

Department of Electrical and Computer Engineering, McGill University, 3480 University Street, Montreal, Quebec, Canada H3A 0E9

ARTICLE INFO

Article history:
Received 18 June 2012
Received in revised form
24 April 2013
Accepted 8 May 2013
Available online 15 May 2013

Keywords:
Multi-carrier modulation
Perfect reconstruction
Uniform DFT modulated filter banks
Paraunitary matrices

ABSTRACT

In this work, we propose a novel method for the design of oversampled perfect reconstruction (PR) discrete Fourier transform (DFT) modulated filter banks (FB) for application to multi-carrier modulation (MCM). The PR property is enforced by employing a parametric class of paraunitary matrices to form the transmit/receive polyphase filters of the transceiver system. Specifically, the polyphase filters are formed by cascading special types of paraunitary matrices characterized by a limited set of design parameters. To reduce the number of these parameters, three different factorization methods are employed and compared. Through the optimization of these design parameters, the stop-band energy of the subband filters can be minimized which leads to improved spectral containment. The performance of the proposed system is investigated in a multi-carrier transceiver application, where it is compared with OFDM and other recently proposed FB structures. Numerical results show that the proposed scheme leads to a clear advantage not only in additive white Gaussian noise (AWGN) and frequency selective channels, but also in the presence of channel impairments such as narrow band interference or carrier frequency offset. In particular, it is found that a significant reduction in the bit error rate can be achieved by employing the proposed scheme.

1. Introduction

Multi-carrier modulation (MCM) is an efficient transmission technique for high data rate wired and wireless communications, where the channel bandwidth is divided into several subchannels with their own carriers. There are many different possible realizations for MCM systems, but with no doubt, orthogonal frequency division multiplexing (OFDM) [1] has been the most prevalent solution in many current standards. From a filter bank perspective, OFDM is based on inverse discrete Fourier transform (IDFT) and discrete Fourier transform (DFT) blocks. As a result, its prototype filters are rectangular windows with poor frequency localization: their magnitude response consists of a mainlobe overlapping with immediate adjacent subchannels and high sidelobes that extend over a wide frequency band. Consequently, channel impairments such as narrow band interference (NBI) and carrier frequency offset (CFO) can deteriorate its performance [2–4].

To avoid such drawbacks, filter bank multi-carrier (FBMC) systems have been proposed which benefit from improved frequency selectivity through the use of longer prototype filters [5,6]. FBMC systems consist of a synthesis (transmit) and analysis (receive) filter banks (FB), interconnected by a transmission channel. Denoting M as the number of subbands and K as the upsampling/downsampling factor, the FB is said to be critically sampled if $K=M$ and oversampled if $K>M$, while perfect reconstruction (PR) refers to a condition where the output of the tandem

☆ This work was supported by InterDigital Canada Lte., the Natural Sciences and Engineering Research Council of Canada, and the Government of Quebec under the PROMPT program.

* Corresponding author. Tel.: +1 5143985701.
E-mail addresses: siavash.rahimi@mail.mcgill.ca (S. Rahimi), benoit.champagne@mcgill.com (B. Champagne).

0165-1684/$ - see front matter © 2013 Elsevier B.V. All rights reserved.
http://dx.doi.org/10.1016/j.sigpro.2013.05.003

combination of the transmit and receive FBs is a delayed version of the input [5]. Compared to critically sampled FBs, oversampled FBs benefit from additional design freedom that can be used to obtain the PR property *and* additional spectral containment, hence better noise immunity [6–10]. These improvements come at the cost of increased redundancy and loss of spectral efficiency.

To reduce design and implementation complexity, DFT modulated FBs are commonly used as a computationally efficient solution in the practical application of FBMC systems [7–16]. In this approach, the M transmit and M receive subband filters are all derived from a single prototype filter, typically a finite impulse response (FIR) filter of length D, so that the total number of design parameters is significantly reduced.

One common realization of FBMC systems is OFDM/OQAM systems that use offset-quadrature amplitude modulation (OQAM), instead of common quadrature amplitude modulation (QAM) signaling, in order to maintain orthogonality between adjacent subbands [11–14]. This requires employing OQAM pre- and post-processing blocks in the transmitter and receiver, so that only pure real or imaginary signals are fed to the subband filters, which also adds to the system complexity and makes the channel estimation difficult. The implementation of such systems in MIMO scenarios also poses a practical difficulty, in that the Alamouti scheme cannot be directly applied to it.

Alternatively, considering that non-ideal channels will introduce distortion and prevent the PR of the transmitted signal, some researchers have investigated the design of nearly-perfect reconstruction (NPR) FBs for MCM applications [17,18], where small amounts of inter-symbol interference (ISI) and ICI are present even in the ideal channel case. In practice, the level of these interferences can be controlled through optimization of the analysis/synthesis filters and kept small compared to the distortion inflicted by the channel on the demodulated signals. In [18], a windowing method for the design of NPR systems is proposed that can reduce the number of design parameters considerably. This method employs a class of prototype filters closely related to the so-called Nyquist filters [19]. Compared to the simple one-tap per subband equalizers for PR systems, NPR design entails the use of more complex equalizers at the receiver to combat ISI, which adds to the system's complexity [20].

Motivated by the above considerations, the focus in this work is on the application of oversampled PR (OPR) DFT modulated (DFTM) FBs to MCM systems. In this regard, to reduce realization complexity and simplify design, it is of great importance to provide an efficient structure based on a minimum number of elementary building blocks, i.e. delay and rotation matrices. The first attempts to find an efficient factorization for paraunitary matrices in this field are focused on critically sampled PR FBs and reported in [5,21–23], although they cannot be applied to OPR FBMC systems. Alternatively, in [8], it has been demonstrated that the parameterization of the polyphase matrix for the OPR case can be achieved with different degrees of freedom, i.e. with different numbers of independent rotation parameters, but this approach does not provide a formal construction algorithm and the solution sets are redundant. As a result, in [24], it is shown that by employing a sequence of transformations on these solutions the non-redundant solutions can be extracted. Similarly, using the dyadic-based factorization [25], another design method for OPR DFTM FBs in the context of MCM is presented in [9]. But the size of the associated parameter vector is relatively large, suggesting that this method can be further improved. Recently, in [16], we provided a detailed factorization for the polyphase matrix of OPR DFTM FBs using elementary building blocks, including Givens rotations and delay matrices. However, with this method, increasing the number of subbands makes the design process tedious due to the still large number of parameters.

In this paper, we propose an efficient factorization method to design OPR DFTM FBMC transceivers. The PR property is enforced by employing a parametric class of elementary paraunitary transformations to form the polyphase filtering matrices of the transmit and receive sub-systems. Different parameterization methods for paraunitary matrices are applied to enforce OPR requirements and then compared in terms of number of parameters. By employing the *Hermitian unitary* and *post-filtering* methods of paraunitary matrices [22,23], we are able to reduce the number of representation parameters compared to the approach in [9,16] and as a result, the design process is faster and less complex. In turn, the prototype filter coefficients of the analysis/synthesis banks can be naturally expressed in terms of the entries of these paraunitary polyphase matrices, allowing for a complete yet efficient parameterization of the desired OPR DFTM FB. The FBMC design is formulated as a minimization problem over the new parameter space, where the objective function is the stop-band attenuation of the subband filters. The resulting prototype filters benefit from excellent spectral containment, i.e. high stop-band attenuation and sharp transition band. The bit error rate (BER) performance of the proposed FBs in MCM transceiver applications is evaluated via extensive computer experiments in frequency selective and AWGN channels. The result shows increased immunity of the new system against NBI and colored noise, as compared to OFDM. Furthermore, because it employs sharp filters with much lower sidelobes, the proposed transceiver structure outperforms ODFM. The counterpart for these appealing properties is an increase in the computational complexity and processing delay of the system.

The paper is organized as follows. The MCM system model under study and the associated design problem are exposed in Section 2. A convenient decomposition of the polyphase filtering matrices of the transmit and receive sub-systems into main paraunitary factors is developed in Section 3. In Section 4, the final parameterization of the polyphase matrices is achieved through a further decomposition of one of these factors into elementary paraunitary building blocks. The design of the resulting OPR DFTM FBs through optimization of their parameters is presented in Section 5, along with design examples of prototype filters. Experimental results of the proposed OPR DFTM FBMC transceivers are investigated through numerical simulations under different channel and interference conditions in Section 6. Finally, Section 7 concludes the work.

Notations: Bold-faced letters indicate vectors and matrices, e.g. $\mathbf{A}$. The (i,j)th entry of a matrix is represented by $[\mathbf{A}]_{i,j}$. The superscripts T and H stand for the transpose

and Hermitian transpose of a vector or matrix, respectively, while the superscript $*$ denotes complex conjugation. $\mathbf{I}_K$ and $\mathbf{0}_{K\times M}$, respectively, denote the $K\times K$ identity matrix and $K\times M$ zero matrix. The paraconjugate operation on a matrix function $\mathbf{E}(z)$ is defined by $\tilde{\mathbf{E}}(z)=\mathbf{E}(1/z^*)^H$. A $M\times K$ matrix function $\mathbf{E}(z)$ is said to be paraunitary if $\tilde{\mathbf{E}}(z)\mathbf{E}(z)=c\mathbf{I}_K$, where $c>0$ is a constant. $\lfloor x\rfloor$ and $\lceil x\rceil$ denote the integer floor and ceiling of x. Finally, a is congruent to b modulo m, or $a\equiv b(\mathrm{mod}\ m)$, whenever $a-b$ is divisible by m.

2. Background and problem formulation

The FBMC transceiver system under consideration is depicted in Fig. 1, where integer parameters M and K represent the number of subbands and the upsampling factor, respectively; as explained before, we consider oversampled FBs, where $K>M$. Let $x_i[n]$ denote the complex-valued data sequence transmitted on the ith subband, $i\in\{0,\ldots,M-1\}$, where $n\in\mathbb{Z}$ is the discrete-time index at the low sampling rate F_s. Sequence $x_i[n]$ is expanded by a factor of K and then passed through its corresponding subband filter with system function $F_i(z)=\sum_{m\geq 0}f_i[m]z^{-m}$, where $f_i[m]$ denotes the filter impulse response and $z\in\mathbb{C}$. The filtered signals are then added together to form the transmitter output $y[m]$, where $m\in\mathbb{Z}$ is the discrete-time index at the high sampling rate KF_s:

$$y[m]=\sum_{i=0}^{M-1}\sum_{n=-\infty}^{\infty}f_i[m-nK]x_i[n]. \tag{1}$$

In an actual implementation, $y[m]$ would be D/A converted and modulated for transmission over a desired frequency band, followed by demodulation and A/D conversion on the receiver side; here, we focus on a baseband representation of these operations which is equivalent from a signal processing viewpoint. The physical transmission channel (including transmitter back-end and receiver front-end) is modeled as a linear time-invariant discrete-time filter with finite impulse response (FIR) $c[m]$ and corresponding system function $C(z)=\sum_{m=0}^{Q-1}c[m]z^{-m}$, where positive integer Q denotes the filter length. During its transmission, signal $y[m]$ is corrupted by various additive perturbation sources (radio interference, cross-talk, thermal noise, etc.). Accordingly, the channel output is expressed as

$$\hat{y}[m]=\sum_{l=0}^{Q-1}c[l]y[m-l]+\eta[m]+\beta[m] \tag{2}$$

where $\eta[m]$ is modeled as a (zero-mean) additive white Gaussian noise (AWGN) process and $\beta[m]$ denotes other possible interferences.

In the receiver, the ith subband signal $\hat{x}_i[n]$ is recovered by passing the channel output $\hat{y}[m]$ through a corresponding subband filter with system function $H_i(z)=\sum_{m\geq 0}h_i[m]z^m$, where $h_i[m]$ denotes the (time-reversed) impulse response (For convenience in analysis, $H_i(z)$ is assumed to be non-causal; in practice, causality can be restored simply by introducing an appropriate delay in the receiver.), and decimating the result by a factor of K:

$$\hat{x}_i[n]=\sum_{m=-\infty}^{\infty}h_i[m-nK]\hat{y}[m]. \tag{3}$$

In DFTM FBs, the transmit and receive subband filters are derived from common prototype filters, typically of the FIR type with system functions $F_0(z)=\sum_{n=0}^{D-1}f_0[n]z^{-n}$ and $H_0(z)=\sum_{n=0}^{D-1}h_0[n]z^n$, respectively, where D is the common filter length. In this work, D is restricted to be a multiple of M and K, i.e. $D=d_MM=d_KK$, where d_M and d_K are positive integers. Denoting by P the least common multiple of M and K, we can also write $D=d_PP$ and $P=p_MM=p_KK$, with d_P, p_M and p_K integers. Defining $w=e^{-j2\pi/M}$, the system functions of the transmit and receive filters for the ith subband are, respectively, obtained as

$$F_i(z)=F_0(zw^i)=\sum_{n=0}^{D-1}f_0[n]w^{-in}z^{-n}, \tag{4}$$

$$H_i(z)=H_0(zw^i)=\sum_{n=0}^{D-1}h_0[n]w^{in}z^{n}. \tag{5}$$

Let us consider the K-fold polyphase representation of the ith transmit filter $F_i(z)$:

$$F_i(z)=\sum_{r=0}^{K-1}z^{-r}P_{i,r}(z^K), \tag{6}$$

$$P_{i,r}(z)=\sum_{n=0}^{d_K-1}f_0[Kn+r]w^{-i(Kn+r)}z^{-n}. \tag{7}$$

We define the $K\times M$ transmit polyphase matrix $\mathbf{P}(z)$, with entries $[\mathbf{P}(z)]^{r,i}=P_{i,r}(z)$ for $r\in\{0,\ldots,K-1\}$ and $i\in\{0,\ldots,M-1\}$. Similarly, the ith receive filter $H_i(z)$ admits the polyphase representation

$$H_i(z)=\sum_{r=0}^{K-1}z^{r}R_{i,r}(z^K), \tag{8}$$

$$R_{i,r}(z)=\sum_{n=0}^{d_K-1}h_0[Kn+r]w^{i(Kn+r)}z^{n}. \tag{9}$$

We also define the $M\times K$ receive polyphase matrix $\mathbf{R}(z)$, with entries $[\mathbf{R}(z)]_{i,r}=R_{i,r}(z)$. Using the above polyphase matrix representations in combination with Noble identities [5], the FB transceiver structure in Fig. 1 can be represented as shown in Fig. 2.

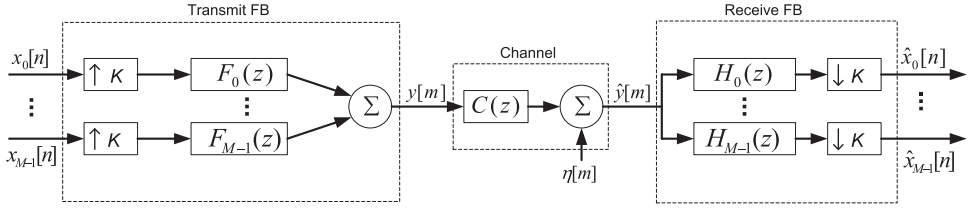

Fig. 1. Oversampled FB transceiver.

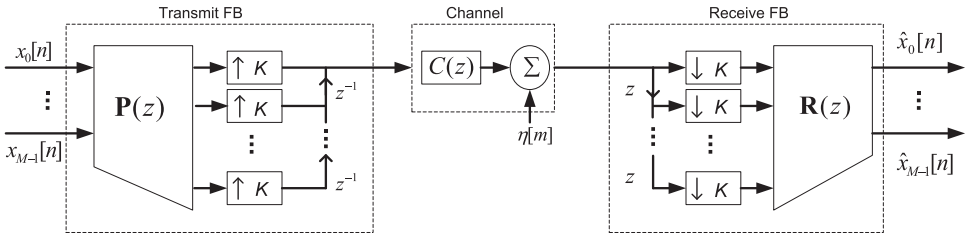

Fig. 2. Oversampled DFTM FB transceiver in polyphase representation.

To ensure that transmission is free from ISI and ICI, the prototype filter characteristics are often chosen to satisfy a PR constraint [7–9], where in the case of an ideal channel (i.e. $C(z)=1$, $\eta[m]=0$ and $\beta[m]=0$), the PR conditions is stated as $\hat{x}_i[n]=cx_i[n]$ for all $i\in\{0,\ldots,M-1\}$ and $n\in\mathbb{Z}$, where c is a constant. Alternatively, this can be expressed in terms of the transmit and receive polyphase matrices as [8]

$$\mathbf{R}(z)\mathbf{P}(z)=c\mathbf{I}_M. \tag{10}$$

In this work, we consider that the transmit and receive prototype filters are paraconjugate of each other, i.e. $H_0(z)=\tilde{F}_0(z)$ or equivalently, $h_0[n]=f_0^*[n]$. Selecting the receive prototype filter in this way implies that the polyphase matrices of the transmit and receive FBs are also paraconjugate, i.e., $\mathbf{R}(z)=\tilde{\mathbf{P}}(z)$ [5]. Consequently, if $\mathbf{P}(z)$ can be made paraunitary, then the PR property of the transceiver system will be achieved since $\mathbf{R}(z)\mathbf{P}(z)=\tilde{\mathbf{P}}(z)\mathbf{P}(z)=c\mathbf{I}_M$. In this case, and assuming an ideal channel, the output of each subband on the receiver side will be a scaled replica of the corresponding subband input on the transmitter side, or $\hat{x}_i[n]=cx_i[n]$.

In addition to guaranteeing the PR property of the system, there are numerous advantages for choosing paraunitary FBs as above [5]: no matrix inversion is required in the design; the transmit and receive filters are FIR with the same length, and can be obtained by time-reversal and conjugation of each other (paraconjugate operator); the passband region of the prototype filter's magnitude response is constant and the objective function does not have to explicitly include passband error. Within this framework, the main problems addressed in this paper can be stated as follows:

(1) To find an efficient parameterization of the prototype filter coefficients $f_0[n]$, in terms of a parameter vector $\boldsymbol{\theta}$ with reduced dimensionality, such that the transmit and receive polyphase matrices are paraunitary and the resulting FBs benefits from the PR property (10); and
(2) Through the choice of a suitable objective function and its optimization over the parameter space, to design improved OPR DFTM FBs for applications to broadband multi-carrier transmissions under practical impairments.

3. A factorization of polyphase matrix P(z)

In this section, the polyphase matrix of the OPR DFTM FB, $\mathbf{P}(z)$, is decomposed into paraunitary factors to establish the PR property. First, we factorize the DFT matrix out of $\mathbf{P}(z)$ and highlight that the remaining matrix term, denoted $\mathbf{U}(z)$, should be paraunitary as well. Next, we investigate the structure of $\mathbf{U}(z)$, especially the relationship between its entries and to the desired prototype filter coefficients.

Finally, we explain how to generate a matrix $\mathbf{U}(z)$ with the desired structure in terms of paraunitary building blocks.

3.1. Preliminary factorization of P(z)

We consider the factorization of the polyphase matrices $\mathbf{P}(z)$ (and consequently $\mathbf{R}(z)$) using an approach similar to that in [9,26]. We begin by defining the $M\times M$ DFT matrix $\mathbf{W}$, with entries $[\mathbf{W}]_{i,j}=w^{ij}$, for all $i,j\in\{0,\ldots,M-1\}$. We also define the block matrices $\mathbf{L}_0$ and $\mathbf{L}_1(z)$, of respective sizes $D\times M$ and $K\times D$, as follows:

$$\mathbf{L}_0=[I_M,I_M,\ldots,I_M]^T, \tag{11}$$

$$\mathbf{L}_1(z)=[I_K,z^{-1}I_K,\ldots,z^{-(d_K-1)}I_K]. \tag{12}$$

Considering first the transmit FB, we represent the D coefficients of the prototype filter $F_0(z)$ by means of diagonal matrix

$$\boldsymbol{\Gamma}_f=\mathrm{diag}(f_0[0],\ldots,f_0[D-1]). \tag{13}$$

Then, using the fact that $w^{M+c}=w^c$, we can write $\mathbf{P}(z)$ in a factored form as follows (see Appendix A):

$$\mathbf{P}(z)=\mathbf{L}_1(z)\boldsymbol{\Gamma}_f\mathbf{L}_0\mathbf{W}^*=\mathbf{U}(z)\mathbf{W}^*, \tag{14}$$

where we define

$$\mathbf{U}(z)=\mathbf{L}_1(z)\boldsymbol{\Gamma}_f\mathbf{L}_0. \tag{15}$$

Proceeding as above, the following factorization can be developed for the receive FB:

$$\mathbf{R}(z)=\mathbf{W}\mathbf{L}_0^T\boldsymbol{\Gamma}_h\tilde{\mathbf{L}}_1(z), \tag{16}$$

where $\boldsymbol{\Gamma}_h=\mathrm{diag}(h_0[0],\ldots,h_0[D-1])=\boldsymbol{\Gamma}_f^*$. Therefore, we can write

$$\mathbf{R}(z)=\mathbf{W}\tilde{\mathbf{U}}(z)=\tilde{\mathbf{P}}(z). \tag{17}$$

Finally, since $\mathbf{W}\mathbf{W}^*=M\mathbf{I}_M$, we note from (14) that the paraunitaryness of $\mathbf{P}(z)$ will follow automatically from that of $\mathbf{U}(z)$. That is:

$$\mathbf{R}(z)\mathbf{P}(z)=\mathbf{W}\tilde{\mathbf{U}}(z)\mathbf{U}(z)\mathbf{W}^*=M\mathbf{I}_M \tag{18}$$

if $\tilde{\mathbf{U}}(z)\mathbf{U}(z)=\mathbf{I}_M$.

3.2. Structure of $\mathbf{U}(z)$

In order to fulfil the PR property, the paraunitaryness of $\mathbf{U}(z)$ should be guaranteed in the design process. Thus, the structure of $\mathbf{U}(z)$ will be further examined in this section. We begin by partitioning the $D\times M$ matrix $\mathbf{\Gamma}_f\mathbf{L}_0$ into the following format:

$$\mathbf{\Gamma}_f\mathbf{L}_0=[\mathbf{F}_0^T|\mathbf{F}_1^T|\ldots|\mathbf{F}_{d_K-1}^T]^T, \tag{19}$$

where matrices $\mathbf{F}_n$, $n\in\{0,\ldots,d_K-1\}$, are of size $K\times M$ with entries

$$[\mathbf{F}_n]_{i,r}=\begin{cases} f_0[nK+i], & \text{if } nK+i\equiv r \pmod M\\ 0, & \text{otherwise}\end{cases} \tag{20}$$

Matrix $\mathbf{U}(z)$ (15) can then be expressed as

$$\mathbf{U}(z)=\mathbf{L}_1(z)[\mathbf{F}_0^T|\mathbf{F}_1^T|\cdots|\mathbf{F}_{d_K-1}^T]^T=\sum_{n=0}^{d_K-1}\mathbf{F}_n z^{-n}. \tag{21}$$

Introducing the change of variables $n=qp_K+\alpha$, where $q\in\{0,\ldots,d_P-1\}$ and $\alpha\in\{0,\ldots,p_K-1\}$, we can rewrite $\mathbf{U}(z)$ as

$$\mathbf{U}(z)=\sum_{q=0}^{d_P-1}\sum_{\alpha=0}^{p_K-1}\mathbf{F}_{qp_K+\alpha}\,z^{-qp_K-\alpha}. \tag{22}$$

Noting that $p_KK=P$ and $P\equiv 0 \pmod M$, we obtain from (20) that

$$[\mathbf{F}_{qp_K+\alpha}]_{i,r}=\begin{cases} f_0[qP+\alpha K+i], & \alpha K+i\equiv r \pmod M\\ 0, & \text{otherwise}\end{cases} \tag{23}$$

We note that given a pair of indices (i,r), $[\mathbf{F}_{qp_K+\alpha}]_{i,r}$ is identically zero except possibly for one specific value of $\alpha\in\{0,\ldots,p_K-1\}$ which, if it exists, is denoted as $\alpha_{i,r}$ and satisfies

$$\alpha_{i,r}K+i\equiv r \pmod M. \tag{24}$$

If this is the case, then it follows from (23) and (24) that

$$[\mathbf{U}(z)]_{i,r}=z^{-\alpha_{i,r}}\sum_{q=0}^{d_P-1}f_0[qP+\alpha_{i,r}K+i]z^{-qp_K}; \tag{25}$$

otherwise $[\mathbf{U}(z)]_{i,r}=0$. Finally, by introducing the polynomials

$$G_{i,r}(z)=\sum_{q=0}^{d_P-1}f_0[qP+\alpha_{i,r}K+i]z^{-q}, \tag{26}$$

we can simplify Eq. (25) as

$$[\mathbf{U}(z)]_{i,r}=z^{-\alpha_{i,r}}G_{i,r}(z^{p_K}). \tag{27}$$

3.3. Expressing $\mathbf{U}(z)$ in terms of paraunitary building blocks

Several efficient parameterizations of paraunitary matrices have been developed and studied in the literature. Here, we would like to employ some of these parameterizations to construct matrix $\mathbf{U}(z)$. Unfortunately, the elements of an arbitrarily generated paraunitary matrix, say $\mathbf{B}(z)$, will not in general match the structure of $\mathbf{U}(z)$ in (15). That is, $\mathbf{B}(z)$ must be further restricted such that its components are compatible with $\mathbf{U}(z)$. The exact way of realizing this depends on whether or not M and K are coprime. The details are provided below.

3.3.1. M and K coprime

When M and K are coprime, i.e. when the least common multiple of M and K is their product $P=MK$ [27], we have $p_K=M$ and $p_M=K$ and, consequently, a unique $\alpha_{i,r}$ in (24) exists for all the entries of $\mathbf{U}(z)$. We define two paraunitary matrices $\mathbf{D}_0(z)$ and $\mathbf{D}_1(z)$ as

$$\mathbf{D}_0(z)=\mathrm{diag}(z^{\alpha_{0,0}},z^{\alpha_{1,0}},\ldots,z^{\alpha_{p_M-1,0}}), \tag{28}$$

$$\mathbf{D}_1(z)=\mathrm{diag}(z^{\alpha_{0,0}},z^{\alpha_{0,1}},\ldots,z^{\alpha_{0,p_K-1}}). \tag{29}$$

The entries of the product $\mathbf{D}_0(z)\mathbf{U}(z)\mathbf{D}_1(z)$ can be written as

$$[\mathbf{D}_0(z)\mathbf{U}(z)\mathbf{D}_1(z)]_{i,r}=z^{\alpha_{i,0}+\alpha_{0,r}}[\mathbf{U}(z)]_{i,r}. \tag{30}$$

Using the index pairs $(i,0)$, $(0,r)$, and (i,r) in (24), we can show that $(\alpha_{i,0}+\alpha_{0,r}-\alpha_{i,r})K\equiv 0 \pmod M$. Equivalently, introducing

$$\hat{\alpha}_{i,r}=\alpha_{i,0}+\alpha_{0,r}-\alpha_{i,r}, \tag{31}$$

we have

$$\hat{\alpha}_{i,r}K\equiv 0 \pmod M. \tag{32}$$

Then, by using (27), we can rewrite (30) as

$$[\mathbf{D}_0(z)\mathbf{U}(z)\mathbf{D}_1(z)]_{i,r}=z^{\hat{\alpha}_{i,r}}G_{i,r}(z^{p_K}). \tag{33}$$

Since $0\le\alpha_{i,r}<p_K$, $\hat{\alpha}_{i,r}$ can take only two values, i.e. 0 or p_K. Accordingly, the entries of $\mathbf{D}_0(z)\mathbf{U}(z)\mathbf{D}_1(z)$ are polynomials in z^{p_K}. Let $\mathbf{B}(z)$ be an arbitrary paraunitary matrix $\mathbf{B}(z)$ of order $L-1$ with entries

$$[\mathbf{B}(z)]_{i,r}=\sum_{q=0}^{L-1}b_{i,r}[q]z^{-q}. \tag{34}$$

Then, it follows from (29) and (30) that

$$\mathbf{U}(z)=\tilde{\mathbf{D}}_0(z)\mathbf{B}(z^{p_K})\tilde{\mathbf{D}}_1(z), \tag{35}$$

$\mathbf{U}(z)$ will be paraunitary as well and the PR condition will be satisfied.

Hence, each entry of $\mathbf{U}(z)$ can be represented in terms of the corresponding entry of $\mathbf{B}(z)$ as

$$[\mathbf{U}(z)]_{i,r}=z^{-(\alpha_{i,0}+\alpha_{0,r})}[\mathbf{B}(z^{p_K})]_{i,r} \tag{36}$$

Clearly, this will be consistent with (28) if the following identity is satisfied:

$$[\mathbf{B}(z^{p_K})]_{i,r}=z^{\hat{\alpha}_{i,r}}G_{i,r}(z^{p_K})=z^{\hat{\alpha}_{i,r}}\sum_{q=0}^{d_P-1}f_0[qP+\alpha_{i,r}K+i]z^{-qp_K} \tag{37}$$

which is the desired equation linking the prototype filter coefficients to the entries of an arbitrary paraunitary matrix. Depending on the value of $\hat{\alpha}_{i,r}$, the coefficients of the prototype filter for $i\in\{0,\ldots,K-1\}$, $r\in\{0,\ldots,M-1\}$, and $q\in\{0,\ldots,d_P-2\}$, can be retrieved as

$$\hat{\alpha}_{i,r}=0\Longrightarrow\begin{cases} f_0[qP+\alpha_{i,r}K+i]=b_{i,r}[q]\\ f_0[D-P+\alpha_{i,r}K+i]=0\end{cases} \tag{38}$$

$$\hat{\alpha}_{i,r}=p_K\Longrightarrow\begin{cases} f_0[(q+1)P+\alpha_{i,r}K+i]=b_{i,r}[q]\\ f_0[\alpha_{i,r}K+i]=0\end{cases} \tag{39}$$

where some of the prototype filter coefficients are preassigned to zero based on (37).[1] Moreover, the proper

[1] The assignments of these coefficients to zero explains the different ranges of variation for q in (37)–(39).

value of L, corresponding to the matrix $\mathbf{B}(z)$, can be determined to be $L=d_P-1$ such that there is enough entries to derive all the remaining prototype filter coefficients and preserve the PR property of the system.

3.3.2. M and K non-coprime

In this case, we can not find the proper $\alpha_{i,r}$ that satisfy (24) for some pairs (i,r). Thus, the resulting $\mathbf{U}(z)$ consists of zero and non-zero entries. Let τ denote the greatest common divisor of K and M, i.e. $\tau=KM/P$. For $l\in\{0,\ldots,\tau-1\}$, we define the $p_M\times p_K$ submatrices $\mathbf{U}_l(z)$ in terms of entries of $\mathbf{U}(z)$ as

$$[\mathbf{U}_l(z)]_{a,b}=[\mathbf{U}(z)]_{l+a\tau,l+b\tau}, \tag{40}$$

where $a\in\{0,\ldots,p_M-1\}$, $b\in\{0,\ldots,p_K-1\}$ and the entries of $\mathbf{U}(z)$ are provided by (25). According to [28], the paraunitaryness of $\mathbf{U}_l(z)$ for $l\in\{0,\ldots,\tau-1\}$ guarantees the paraunitaryness of $\mathbf{U}(z)$. It is straightforward to show that for $i=l+a\tau$ and $r=l+b\tau$, the congruence relation (24) can be simplified to

$$\alpha_{l+a\tau,l+b\tau}p_M+a\equiv b \pmod{p_K}. \tag{41}$$

Because p_K and p_M are coprime, the $p_M\times p_K$ submatrices $\mathbf{U}_l(z)$ can now be expressed in a similar fashion as in the previous subsection, i.e. (36). Specifically, let $\mathbf{B}_l(z)$ for $l\in\{0,\ldots,\tau-1\}$ be arbitrary paraunitary matrices of size $p_M\times p_K$. Each one of these matrices can be mapped to its corresponding FB polyphase submatrix $\mathbf{U}_l(z)$ through the following transformation:

$$\mathbf{U}_l(z)=\tilde{\mathbf{D}}_0(z)\mathbf{B}_l(z^{p_K})\tilde{\mathbf{D}}_1(z). \tag{42}$$

Note that when M and K are non-coprime, τ different matrices $\mathbf{B}_l(z)$ should be generated.

4. Choice of a parameterization for paraunitary matrix B(z)

In this section, different approaches to parameterize a paraunitary matrix are investigated and compared to find the most efficient way to build matrix $\mathbf{B}(z)$ in the coprime case (34) or matrices $\mathbf{B}_l(z)$ for $l\in\{0,\ldots,\tau-1\}$ in the non-coprime case (42).[2] To this end, a constructive procedure for factoring a paraunitary polynomial matrix $\mathbf{B}(z)$ with order $L-1$ as a product of elementary paraunitary matrices is required.

A basic approach for the factorization of paraunitary matrix with constrained filter length is proposed in [21]. By employing this *order-based* method, any paraunitary matrix of order $L-1$ can be factorized into a product of $L-1$ order-one building blocks. This method is implemented in [16] to parameterize the polyphase matrix for design of real prototype filters of OPR DFTM FB. The completeness[3] of this order-based method is proved in [22], where it is developed into a more efficient structure based on the cosine–sine (CS) decomposition of Hermitian unitary matrices. As a result, compared to the order-based method in [21], the authors of [22] are able to reduce the number of free parameters by half in their method, denoted as cosine–sine decomposition *(CSD)-based* method here. However, as noted in [23], even though being complete and minimal,[4] the CSD-based method involves redundant parameterized subsets. Thus, by consecutive removal of extra degrees of freedom in adjacent stages, another factorization method, denoted as *post-filtering based* method, is developed in [23], which can further reduce the number of parameters. Here, we develop these three parametrization methods, namely order-based, CSD-based and post-filtering based, and then compare them in terms of number of parameters required to represent a arbitrary paraunitary matrix.

4.1. Order-based method

We first generate a square $p_M\times p_M$ paraunitary matrix $\mathbf{\Delta}(z)$, then apply the transformation

$$\mathbf{B}(z)=\mathbf{\Delta}(z)\mathbf{\Upsilon}, \tag{43}$$

where $\mathbf{\Upsilon}^T=[\mathbf{I}_{p_K},\mathbf{0}_{p_K\times(p_M-p_K)}]$. With regard to $\mathbf{\Delta}(z)$, the decomposition for an $p_M\times p_M$ paraunitary matrix in terms of order-one paraunitary matrices as in [5,21] is used. For a paraunitary matrix of order $L-1$, this decomposition can be written in terms of delay matrices and unitary matrices as follows:

$$\mathbf{\Delta}(z)=\mathbf{R}_{L-1}\mathbf{\Lambda}(z)\mathbf{R}_{L-2}\mathbf{\Lambda}(z)\ldots\mathbf{R}_0, \tag{44}$$

where $\mathbf{\Lambda}(z)$ is a delay matrix

$$\mathbf{\Lambda}(z)=\mathrm{diag}(\mathbf{I}_{p_M-r_c},z^{-1}\mathbf{I}_{r_c}), \tag{45}$$

with $r_c=\lfloor p_M/2\rfloor$ and $\mathbf{R}_j$ is a unitary product of $p_M(p_M-1)/2$ Givens rotation matrices [29]:

$$\mathbf{R}_j=\prod_{p=0}^{p_M-1}\prod_{q=p+1}^{p_M-1}\mathbf{G}_{p,q}(\theta_{p,q}^j) \tag{46}$$

For each real Givens rotation matrix $\mathbf{G}_{p,q}(.)$, one parameter $\theta_{p,q}^j$ is required [30]. Due to the fact that there are $p_M(p_M-1)/2$ different off-diagonal positions above the diagonal, the number of parameters $\mu_r^{(1)}$ required to construct a $p_M\times p_M$ real paraunitary matrix as in (44) is

$$\mu_r^{(1)}=Lp_M(p_M-1)/2. \tag{47}$$

Recall that the factorization of $\mathbf{B}(z)$ is performed to obtain the parameterized prototype filter coefficients. By using the real Givens rotation matrices, all the coefficients of the resulting prototype filter will be real. Since DFTM FBs are being utilized, there is no advantage in employing real prototype filters in terms of implementation cost, while prototype filters with complex coefficients may benefit from better spectral containments. Therefore, by using complex Givens rotation matrices, we can remove this constraint and assess the characteristics of the resulting complex prototype filters compared to the real ones. Note that for each complex Givens rotation matrix two arbitrary rotation angles are needed, say θ_1 and θ_2, where a

[2] To simplify the presentation, we use the same notation, $\mathbf{B}(z)$, for both cases.

[3] A paraunitary factorization is said to be complete if any paraunitary matrix can be factorized in that form.

[4] A structure (or implementation or realization) is said to be minimal if the number of delay elements is the smallest possible.

2×2 complex Givens rotation matrix is given by

$$\begin{bmatrix} \cos\theta_1 & e^{j\theta_2}\sin\theta_1 \\ -e^{-j\theta_2}\sin\theta_1 & \cos\theta_1 \end{bmatrix} \tag{48}$$

Note that the real Givens rotation matrix is obtained by setting $\theta_2=0$ in (48). Similar to the real case, $\mu_c^{(1)}$ denotes the number of parameters to construct a $p_M\times p_M$ complex paraunitary matrix as

$$\mu_c^{(1)}=Lp_M(p_M-1). \tag{49}$$

4.2. CSD-based method

In [22], based on the singular value decomposition (SVD) of coefficient matrices of $\mathbf{\Delta}(z)$, it was proved that (44) is complete and any paraunitary matrix $\mathbf{\Delta}(z)$ can be represented via (44). However, due to the highly nonlinear relation between the rotation angles in (44)–(46) and the resulting coefficients of matrix $\mathbf{B}(z)$, it is reasonable to characterize it with fewer parameters and reduce the optimization complexity. In [22], it has been shown that there are some redundancies in the representation (44)–(46) of $\mathbf{\Delta}(z)$ and that the number of required parameters can indeed be reduced. Specifically, (44) can be factored as

$$\mathbf{\Delta}(z)=\overline{\mathbf{R}}_{L-1}(z)\overline{\mathbf{R}}_{L-2}(z)\ldots\mathbf{R}_0, \tag{50}$$

where $\overline{\mathbf{R}}_l(z)$, which stands for the product $\mathbf{R}_l\mathbf{\Lambda}(z)$, takes the form

$$\overline{\mathbf{R}}_l(z)=\frac{1}{2}(\mathbf{I}+\mathbf{A}_l)+\frac{1}{2}(\mathbf{I}-\mathbf{A}_l)z^{-1}. \tag{51}$$

In this representation, $\mathbf{A}_l$ is a Hermitian unitary matrix with the special structure

$$\mathbf{A}_l=\mathrm{diag}(\mathbf{V}_l,\mathbf{W}_l)\mathbf{Q}_l\mathbf{\Gamma}_l\mathbf{Q}_l\,\mathrm{diag}(\mathbf{V}_l^H,\mathbf{W}_l^H), \tag{52}$$

where, $\mathbf{V}_l$ and $\mathbf{W}_l$ are $\lfloor p_M/2\rfloor\times\lfloor p_M/2\rfloor$ and $\lceil p_M/2\rceil\times\lceil p_M/2\rceil$ unitary matrices, respectively, $\mathbf{\Gamma}_l$ is a diagonal matrix with diagonal entries ± 1 (i.e., exactly r_c of these entries are equal to -1 with $\binom{p_M}{r_c}$ combinations), and $\mathbf{Q}_l$ is a real orthogonal matrix of the form

$$\mathbf{Q}_l=\begin{cases}\begin{bmatrix}\hat{\mathbf{C}}_l & \hat{\mathbf{S}}_l\\ \hat{\mathbf{S}}_l & -\hat{\mathbf{C}}_l\end{bmatrix}, & \text{for even } p_M\\ \begin{bmatrix}\hat{\mathbf{C}}_l & 0 & \hat{\mathbf{S}}_l\\ 0 & \pm 1 & 0\\ \hat{\mathbf{S}}_l & 0 & -\hat{\mathbf{C}}_l\end{bmatrix}, & \text{for odd } p_M\end{cases} \tag{53}$$

In (53), $\hat{\mathbf{C}}_l$ and $\hat{\mathbf{S}}_l$ are $\lfloor p_M/2\rfloor\times\lfloor p_M/2\rfloor$ real diagonal matrices with entries $[\hat{\mathbf{C}}_l]_{n,n}=\cos(\alpha_{l,n})$ and $[\hat{\mathbf{S}}_l]_{n,n}=\sin(\alpha_{l,n})$.

We note that with CSD-based method as explained above and using real Givens rotations to obtain $\mathbf{V}_l$ and $\mathbf{W}_l$, the coefficients or the entries of $\mathbf{B}(z)$ and the resulting prototype filter's coefficients will be real. Alternatively, by using complex Givens rotation matrices for $\mathbf{V}_l$ and $\mathbf{W}_l$, complex prototype filters can be derived. The numbers of required parameters to generate $\mathbf{\Delta}(z)$ by this approach (50)–(53) are $\mu_r^{(2)}$ and $\mu_c^{(2)}$ for the real and complex cases, respectively.

$$\mu_r^{(2)}=(L-1)(\lfloor p_M/2\rfloor(\lfloor p_M/2\rfloor-1)/2 + \lceil p_M/2\rceil(\lceil p_M/2\rceil-1)/2+\lfloor p_M/2\rfloor)+p_M(p_M-1)/2 \tag{54}$$

$$\mu_c^{(2)}=(L-1)(\lfloor p_M/2\rfloor(\lfloor p_M/2\rfloor-1)+\lceil p_M/2\rceil(\lceil p_M/2\rceil-1) + \lfloor p_M/2\rfloor)+p_M(p_M-1) \tag{55}$$

Note that these values are almost half of the number of parameters used in the order-based method (44).

4.3. Post-filtering based method

In [23], the authors developed an algorithm called post-filtering based method and further reduced the number of required parameters. By consecutive removal of extra degrees of freedom in adjacent stages, which is accomplished through a new CS decomposition and implementing a post-filtering based structure, they succeeded in eliminating redundant parameters. This structure is derived by forward simplification of (44) as follows:

$$\mathbf{\Delta}(z)=\hat{\mathbf{R}}_{L-1}\mathbf{\Lambda}(z)\hat{\mathbf{R}}_{L-2}\mathbf{\Lambda}(z)\ldots\mathbf{R}_0, \tag{56}$$

where

$$\hat{\mathbf{R}}_l=\mathrm{diag}(\mathbf{V}_{l,0},\mathbf{V}_{l,1})\mathbf{\Sigma}_l, \tag{57}$$

in which, $\mathbf{V}_{l,0}$ and $\mathbf{V}_{l,1}$ are special $(p_M-r_c)\times(p_M-r_c)$ and $r_c\times r_c$ unitary matrices, respectively. In particular, by absorbing extra parameters into $\hat{\mathbf{R}}_{l-1}$, $\mathbf{V}_{l,0}$ requires $(p_M-2r_c)(p_M-2r_c-1)/2$ fewer parameters than a unitary matrix of a same size in the real case [23]. Likewise, in the complex case, there is a reduction of $(p_M-2r_c)(p_M-2r_c-1)$ in the number of design parameters. Moreover, when $2r_c<p_M$, $\mathbf{\Sigma}_l$ is a $p_M\times p_M$ matrix that can be expressed as

$$\mathbf{\Sigma}_l=\begin{bmatrix}\mathbf{I} & 0 & 0\\ 0 & \mathbf{C}_l & -\overline{\mathbf{S}}_l\\ 0 & \overline{\mathbf{S}}_l^H & \mathbf{C}_l\end{bmatrix}, \tag{58}$$

where, $\mathbf{C}_l$ and $\overline{\mathbf{S}}_l$ are $r_c\times r_c$ diagonal matrices with entries $[\mathbf{C}_l]_{n,n}=\cos(\alpha_{l,n})$ and $[\overline{\mathbf{S}}_l]_{n,n}=e^{j\beta_{l,n}}\sin(\alpha_{l,n})$, where $\alpha_{l,n}$ is a rotation angle and $\beta_{l,n}$ is a phase. Similarly, when $2r_c>p_M$, another CS decomposition is derived for $\mathbf{\Sigma}_l$ in [23]. But as r_c corresponds to the number of delay elements z^{-1} in $\mathbf{\Lambda}(z)$, it is preferable to choose $r_c\le p_M/2$, while it does not violate the completeness of (56). In this case $2r_c<p_M$, the numbers of parameters $\mu_r^{(3)}$ and $\mu_c^{(3)}$ required to construct a $p_M\times p_M$ real and complex paraunitary matrix are, respectively,

$$\mu_r^{(3)}=(L-1)[(p_M-r_c)(p_M-r_c-1)/2-(p_M-2r_c)(p_M-2r_c-1)/2 + r_c(r_c-1)/2+r_c]+p_M(p_M-1)/2, \tag{59}$$

$$\mu_c^{(3)}=(L-1)[(p_M-r_c)(p_M-r_c-1)-(p_M-2r_c)(p_M-2r_c-1) + r_c(r_c-1)+2r_c]+p_M(p_M-1). \tag{60}$$

By considering the extra parameters required to form $\mathbf{\Gamma}_l$ in (50), it can be shown that the number of design parameters in the post-filtering method to generate a paraunitary matrix of size p_M is less than or equal to the one in the CSD-based method. Furthermore, the number of parameters μ in the post-filtering based approach (56) is a

Table 1
Size of parameter vector $\boldsymbol{\theta}$ for $M=64$, $K=72$ and $D=1728$.

Method	μ_r for real prototype	μ_c for complex prototype
Dyadic based	$72\times 8=576$	N/A
Order-based (44)	$72\times 8=576$	$144\times 8=1152$
CSD-based (50)	$56\times 8=448$	$108\times 8=864$
Post-filtering based (56)	$44\times 8=352$	$88\times 8=704$

quadratic function of r_c which reaches its maximum at $\lfloor p_M/2 \rfloor$.

Table 1 lists representative sizes of the parameter vectors of different design methods, including the dyadic based method [9,25], the order-based method (44), the CSD-based method (50), and the post-filtering based method (56). These sizes are for real and complex prototype filters of length $D=1728$ in FBMC system with $M=64$ subbands and $K=72$ as upsampling/downsampling factor. These values are derived for $r_c=1$ using (47), (49), (54), (55), (59) and (60) and considering the fact that $\tau=8$ different matrix $\mathbf{B}(z)$ (or $\boldsymbol{\Delta}(z)$) should be constructed. Unfortunately, due to its limitation, the dyadic based method [9,25] cannot be used to design complex prototype filters. Moreover, we note that one of the advantages of the other three methods over the dyadic based method is that the range of the parameters is limited to the interval $[0, 2\pi]$. Finally, compared to the CSD-based method, the post-filtering based method does not use the extra sign parameters. While as in (52), p_M sign parameters are needed for each $\boldsymbol{\Gamma}_l$ in the CSD-based method. Based on the results of Section 3 and by employing the method with the least number of parameters, it will be possible to parameterize $\mathbf{B}(z)$ and perform the optimization on its associated parameters.

5. Prototype filter design

In this Section, the design steps towards the final optimized prototype filter for a given triplet (K,M,D) are discussed. Depending on whether M and K are coprime, the design process starts with generating parameterized paraunitary matrices $\mathbf{B}(z;\boldsymbol{\theta})$ or $\mathbf{B}_l(z;\boldsymbol{\theta})$ for $l\in\{0,\ldots,\tau-1\}$ via the methods explained in Section 4. In particular, the post-filtering based method (56) has been used due to the fact that the required number of parameters to design such matrices by this method is less or equal to the other methods. The entries of these matrices are then mapped to the prototype filter coefficients $f_0[n;\boldsymbol{\theta}]$ using (37) or (42). Finally, based on the vector of parameters $\boldsymbol{\theta}$, these coefficients are optimized according to the design objectives.

5.1. Optimization of prototype filter

The prototype filter coefficients $f_0[n;\boldsymbol{\theta}]$ are optimized with respect to the vector of parameters $\boldsymbol{\theta}$. One of the benefits of using a PR FB transceiver is that in the filter design process, the PR property relaxes any flatness condition on the passband region of the filter. Since the transmit and receive prototype filters are paraconjugate of each other, the pass band region of $|F_0(\omega;\theta)|^2$ is constant, where $F_0(\omega;\boldsymbol{\theta})=\sum_{n=0}^{D-1} f_0[n;\boldsymbol{\theta}]e^{-j\omega n}$ is the discrete-time Fourier transform (DTFT) of $f_0[n;\boldsymbol{\theta}]$ [5]. Therefore, a good spectral containment can be achieved via minimization of the stop-band energy of the filter, denoted as the cost function

$$J(\boldsymbol{\theta})=\frac{1}{2\pi}\int_{\omega_s}^{2\pi-\omega_s}|F_0(\omega;\boldsymbol{\theta})|^2 d\omega, \tag{61}$$

where ω_s is the stop-band angular frequency, given by

$$\omega_s=\frac{\pi}{M} \tag{62}$$

In order to calculate the cost function $J(\boldsymbol{\theta})$ (61) in an efficient way, we employ a FFT-based algorithm as explained in [9]. Since this optimization problem is a large-scale non-linear one, we used the Broyden–Fletcher–Goldfarb–Shanno (BFGS) algorithm [31], which is a quasi-Newton method, for minimizing the cost function.

Alternatively, we can consider the minimax criterion, which aims to minimize the maximum stop-band ripple instead of the stop-band energy. In minimax design the cost function is defined as

$$J(\boldsymbol{\theta})=\max_{\omega\in[\omega_s,2\pi-\omega_s]}|F_0(\omega;\boldsymbol{\theta})|. \tag{63}$$

The magnitude response of the resulting filter is shaped such that the attenuation is almost equiripple on the overall stop-band region. In general, we find that with the minimax criterion, the attenuation is higher near the edge of the stop-band region and the first few sidelobes are lower than with the stop-band energy minimization criterion, whereas it results in increased total stop-band energy.

5.2. Comparison of prototype filters

It is known that for a given number of subbands M, better spectral features are obtained if the upsampling factor K and the length of the prototype filter D are increased [9]. However, higher K will sacrifice the bandwidth efficiency of the system and higher D will increase latency of the system and its computational complexity. These trade-offs must be balanced carefully in order to maintain low latency, low computational complexity, and high bandwidth efficiency while benefiting from good spectral features. In this section, we design a real and complex prototype filter for the transceiver system with $M=64$ subbands, oversampling factor $K=72$, and filter length $D=1728$. It has been observed that due to the completeness of the methods (44), (50), and (56), the resulting prototype filters are almost identical in terms of spectral containment. However as noted in Section 4, the number of parameters in the post-filtering based method (56) is less than the other methods, and consequently, we prefer this method due to its efficient parameterization.

To develop a comprehensive outlook on various FB design and MCM transceiver systems, the real and complex prototype filters designed by means of the objective function in (61) are compared with the prototype filters of some other design methods including NPR-windowing

using the generalized windowing-based method [18], NPR-OQAM[5] derived by the frequency sampling technique [13] and OFDM. Table 2 lists the filter length D, the stop-band attenuation $J(\boldsymbol{\theta})$ in (61) (when $\omega_s=\pi/M$) and the first sidelobe attenuation of these filters. Moreover, Fig. 3 shows part of the frequency responses (i.e. first few sidelobes) of these filters. Three key observations must be pointed out: the transition from passband to stop-band, i.e. the rolloff, of the proposed scheme is much steeper than all other FB approaches and OFDM; the stop-band energy of the proposed scheme is the second smallest among its counterparts after the NPR-Windowing method; the attenuations of the first two sidelobes of the proposed scheme are, respectively, about 33 and 40 dB, whereas the attenuations of the first two sidelobes of the OFDM system are 13 and 17 dB, respectively. These observations confirm that the proposed OPR FB offer considerably better spectral containment than OFDM.

As mentioned in Section 2, to restore causality in the PR MCM receiver, there is an intrinsic delay in the system that is equal to the prototype filter length D, or equivalently, $D/K=24$ symbol durations at the input rate. The issues faced by our proposed system in the case of burst transmissions, e.g. with regard to the use of a preamble in each burst for channel estimation, are similar to those faced by other FB-based MCM systems [14]. In particular, when accurate estimation is needed, the data should not interfere with the preamble signal and the length of the burst must therefore be extended to allow for initial and final transitions of the preamble due to the filter impulse response. Also, in the case of a time-varying channel, a basic requirement is that the filter length should be smaller than the channel coherence time.

5.3. Prototype filter for $M=128$ and $K=132$

The design of FBMC systems mainly concentrates on the prototype filter design since all the subband filters are generated from this filter. Moreover, practical applications commonly necessitate transceiver structures with high number of subchannels, that is, a value of M in the order of hundreds or thousands is required, e.g. in Digital Video Broadcasting Terrestrial 2 (DVB-T2) application, the number of subcarriers can go up to $M=2^{15}$ [32]. Such a demand imposes a significant computational burden on the conventional design processes as the number of parameters to be optimized may increase drastically or even become overwhelming. As shown for instance in [9,15,16], the number of subbands does not exceed 80, 128, and 64, respectively.

Moreover, when the ratio K/M approaches 1, the number of parameters increases which complicates the optimization process as well. Meanwhile, this case is important in practice since it replaces a more spectral efficient system. The methods presented in the literature only obtained limited success in improving the spectral efficiency, or equivalently, reducing the oversampling ratio K/M. These efforts start with an oversampling ratio of 2 in [33] and continue with values of 3/2 [34] and 5/4 [8,15]. It is only recently that authors in [9,16,24] succeeded in presenting a 9/8, 9/8 and 17/16 oversampling ratio FBMC design, respectively. Benefiting from effective factorization and efficient parameterization, we are able to design real prototype filters with oversampling ratio of 33/32. Based on stop-band energy minimization and minimax criterion, the magnitude responses of these prototype filters for $M=128$ and $K=132$ (oversampling ratio 33/32) are depicted in Fig. 4. The lengths of these filters are $D=12672$ ($D/P=3$) and the size of their parameter vector in the case of a real prototype filter is 560×4 (when using the post-filtering based method with $r_c=1$). Table 3 also lists the stop-band attenuation $J(\boldsymbol{\theta})$ in (61) and the first sidelobe attenuation of these filters. As it is shown in the figure and the table, by employing the minimax criterion we can increase the first sidelobe's attenuation by 4 dB, but this results in increased total stop-band energy. Due to the similar spectral characteristics of the resulting filters, we just focus on the stop-band energy minimization method in the sequel.

6. Numerical results

In this section, the performance of an OPR DFTM FBMC transceiver using the proposed filter bank design approach is investigated through numerical simulations. In particular, the BER of this system when used over a frequency selective channel in the presence of AWGN is compared with other well known MCM schemes. The effects of channel impairments such as CFO and NBI on the BER performance are also examined.

6.1. Methodology

Referring to (2), we consider two different scenarios for the Q-tap channel $C(z)$ with channel coefficients $c[l]$: (1) an ideal (distortion-less) channel for experimenting AWGN, where $Q=1$ and $c[0]=1$ and (2) a frequency selective channel consisting of $Q=5$ independent Rayleigh-fading taps with an exponentially decaying power delay profile, where $E[|c[l]|^2]=Ce^{-l/4}$ for $l\in\{0,\ldots,4\}$, and C is a constant such that $\sum_{l=0}^{Q-1}E[|c[l]|^2]=1$. The received signal includes an additive white Gaussian noise $\eta[m]$ with zero mean and variance $E[|\eta[m]|^2]=N_0$. Moreover, to model a scenario with NBI, a white noise sequence is passed through a narrow band-pass filter with a bandwidth of $2/M$ to generate the narrow band random interference sequence $\beta[m]$. We let $I=E[|\beta[m]|^2]$ denote the interference power. The resulting NBI $\beta[m]$ is then added to the channel output and white Gaussian noise $\eta[m]$ as in (2). This simple interference model is realistic for narrow band FM (eg. cordless telephones) and low rate digital modulations [2,35,36].

To evaluate the comparative performance of the proposed scheme, BERs versus bit-energy-to-noise ratio (E_b/N_0) of the following MCM systems are compared: proposed OPR DFTM FBMC with real prototype filter, proposed OPR DFTM FBMC with complex prototype filter, the NPR-windowing method [18], the NPR-OQAM method [13] designed by criterion C1 in that reference and a cyclic

[5] Most of the literature regarding the OFDM/OQAM system is focused on NPR systems, whereas the PR version is also developed [12].

Table 2
Spectral containment of different prototype filters for $M=64$ subbands.

Method	D	J (dB)	First sidelobe (dB)
Proposed real	1728	−35.31	−33
Proposed complex	1728	−35.29	−33
NPR-windowing [18]	1024	−36.56	−72
NPR-OQAM [13]	255	−26.80	−45
OFDM	64	−24.27	−13

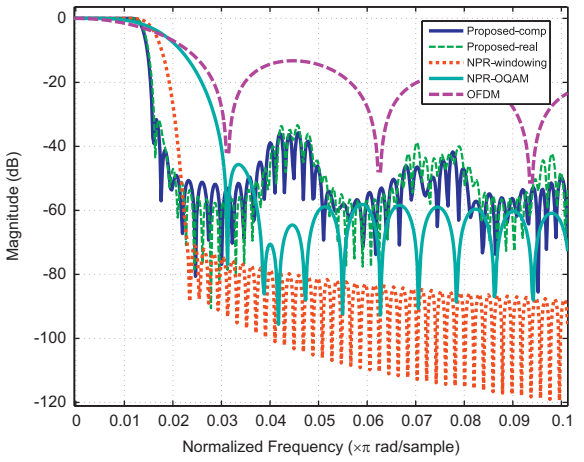

Fig. 3. Comparison of the first few sidelobes of magnitude responses for prototype filter of different design approaches with $M=64$ subbands.

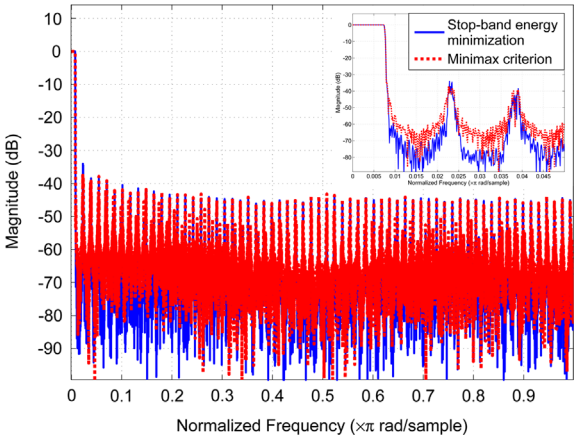

Fig. 4. Magnitude responses of prototype filters for $M=128$ and $K=132$.

Table 3
Spectral containment of prototype filters for $M=128$, $K=132$ and $D=12672$.

Method	J (dB)	First sidelobe (dB)
Stop-band energy	−41.59	−34
Minimax criterion	−40.55	−38

prefix OFDM system. Note that although the NPR schemes are not designed for optimum performance over AWGN channels, it is insightful to compare their behavior in the non-frequency-selective environment as well as in the frequency selective one. For all of these systems, QPSK modulation is used as an input for each subband where the filter bank is normalized to have a DC gain of 1. Furthermore, to derive the BER in each scenario, a number of 10^4 Monte Carlo trials are performed, where the channel is fixed in each run but independent from one run to another. In order to fairly compare these schemes, the redundancy caused by oversampling should be equal to the redundancy caused by the cyclic prefix in OFDM. That is, with $M=64$ and $K=72$, the length of cyclic prefix is set to $L_{cp}=K-M=8$ in OFDM.

Due to the large number of subbands and the excellent spectral characteristics of the prototype filters of the systems under consideration, if the channel is mildly frequency selective, each subband channel can be modelled as a simple (flat) complex gain which can be equalized by a single tap, similar to [37]. As a result, we implement a one-tap equalizer per subband assuming perfect channel state information (CSI), which can be obtained by specialized channel estimation techniques (whose development falls outside the scope of this paper).

The equalizer coefficient for the ith subband is derived as follows:

$$E_i = C(z_i)^{-1}, \tag{64}$$

where $z_i = e^{-j2\pi i/M}$ for $i\in\{0,\ldots,M-1\}$. Unless otherwise indicated, we assume perfect frequency synchronization between the transmit and receive FBs.

6.2. Results and discussion

The computational complexity of FB structures can be evaluated by counting the number of real multiplications needed to compute an output sequence of length-M. This information is reported in Table 4 for the various MCM systems under consideration, assuming a polyphase implementation [14,17], complex-valued data $x_i[n]$, and M a power of 2. As a result, the DFT can be replaced by an FFT, which can be realized more efficiently. As expected, OFDM shows a complexity advantage over the FB approaches as it just employs the IFFT/FFT blocks. The proposed design, in addition to the IFFT/FFT blocks and consistent with other FB methods, employs a polyphase block at the transmitter and receiver where the complexity depends on the prototype filter length. Also, in the case of NPR-OQAM, the IFFT/FFT blocks operate at twice the rate of other systems, and the trivial multiplications by ± 1 and $\pm j$ in the preprocessing blocks are not considered in evaluating the complexity.

The BERs versus E_b/N_0 for the various MCM systems in the ideal AWGN channel environment are plotted in Fig. 5. It can be seen that BER of the FB-based approaches closely match the suggested theoretical value of BER for QPSK and they all exhibit superior performance than OFDM by a margin of 0.5 dB. This difference in BER performance can be precisely explained by the use of a CP with 9/8 redundancy ratio. As we have been able to verify, the BER of OFDM without CP is in full agreement with other methods. In this example, the simulated BER for the real and complex versions of the proposed scheme are almost indistinguishable.

Table 4
Computational complexity in terms of number of real multiplications for systems with M subbands and filter length D.

Method	Number of real multiplications
Proposed	$2((M(\log_2 M-3)+4)+2D)$
NPR-windowing	$2((M(\log_2 M-3)+4)+2D)$
NPR-OQAM	$4(2M+(M(\log_2 M-3)+4)+2D)$
FDM	$2(M(\log_2 M-3)+4)$

With the NPR-windowing method [18], proper demodulation of the received signal over the frequency selective channel requires the use of computationally expensive post combiners to combat the phase rotation caused by non-linear phase channel. As a result, its BER with only one-tap per subband equalizer is much higher than that of the other MCM systems with the same equalization method. Therefore, in all the frequency selective scenarios, the results of the NPR-windowing method are not presented. Fig. 6 shows the BER versus E_b/N_0 of the MCM systems over the frequency selective channel. The proposed schemes exhibit the best performance, followed by NPR-OQAM method at low SNR and OFDM at high SNR. As mentioned before, the performance of the proposed methods and NPR-OQAM can be further improved by utilizing a more complex equalization method. Note that the spectral containment and BER in AWGN and frequency selective channel of the proposed scheme with real and complex prototype filters are almost identical. Therefore, for this particular set-up, there is no clear advantage in using complex prototype filter, although it doubles the number of required parameters in the design process. In the sequel, we just focus our investigation on the case of real prototype filters.

It is well known that the performance of OFDM can be easily impaired by NBI. Due to the better spectral containment of the proposed OPR DFTM FBMC system, as compared to the OFDM, we expect a better performance in the presence of NBI. Fig. 7 shows the BER versus bit-energy-to-NBI ratio (E_b/I) of the mentioned MCM systems, where the Gaussian noise is set to have a SNR of 7 dB. As expected, OFDM exhibits the worst performance due to the low attenuation in the sidelobes, whereas the proposed method provides the best performance and the NPR-OQAM remains very close to it. At low SIR, the performance of the NPR-windowing is worse than the other two FB-based approaches since it employs cosine modulation and real-coefficient prototype filters. The saturation of BER at very high SIR results from the fixed SNR level. Similarly, Fig. 8 shows the BER versus E_b/I in the frequency selective channel, where all the MCM systems exhibit a similar behavior as in the AWGN case and the proposed system offers the best performance over the complete SIR range.

It has been shown that sensitivity to frequency synchronization is one of the disadvantages of OFDM [4]. Small frequency offset in the OFDM receiver results in an attenuation of signal amplitude, loss of orthogonality between subcarriers and consequently intercarrier interference (ICI) from the neighbour subcarriers. The poor spectral containments of the rectangular window of OFDM is the main reason for its performance degradation in the presence of CFO. Similarly, many other MCM schemes may

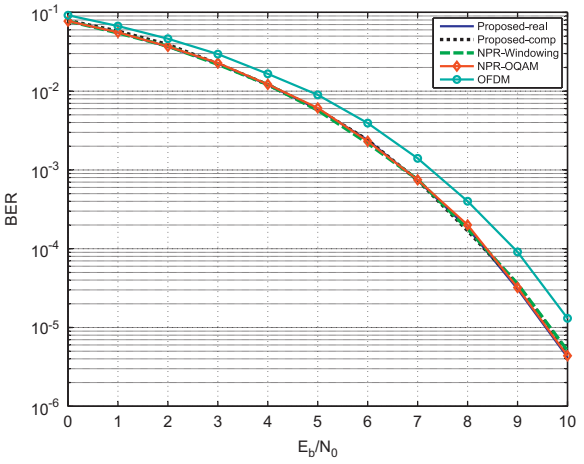

Fig. 5. BER versus E_b/N_0 for different MCM systems with $M=64$ subbands over AWGN channel.

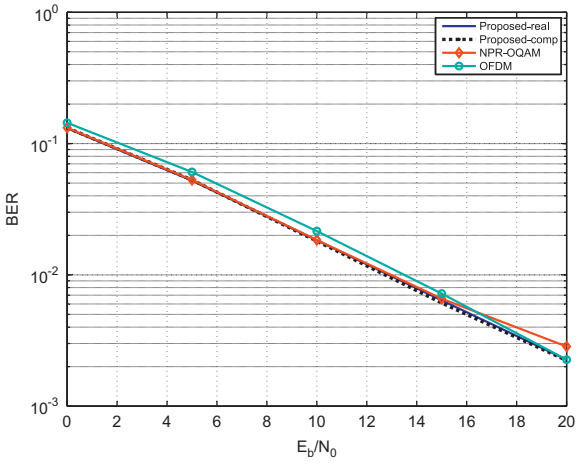

Fig. 6. BER versus E_b/N_0 for different MCM systems with $M=64$ subbands over 5-tap Rayleigh fading channel.

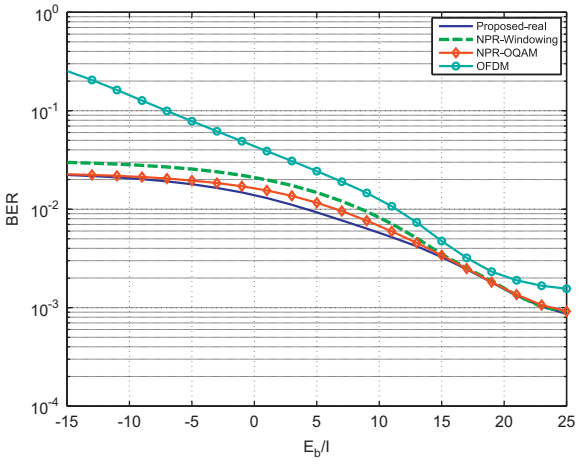

Fig. 7. BER versus E_b/I (NBI) for different MCM systems with $M=64$ subbands over AWGN channel with SNR=7 dB.

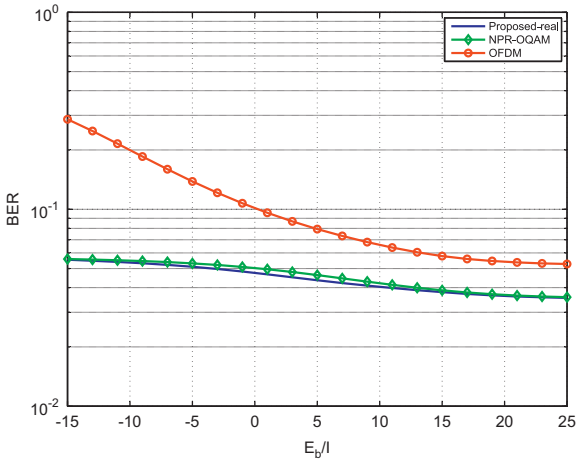

Fig. 8. BER versus E_b/I (NBI) for different MCM systems with $M=64$ subbands over 5-tap Rayleigh fading channel with SNR=7 dB.

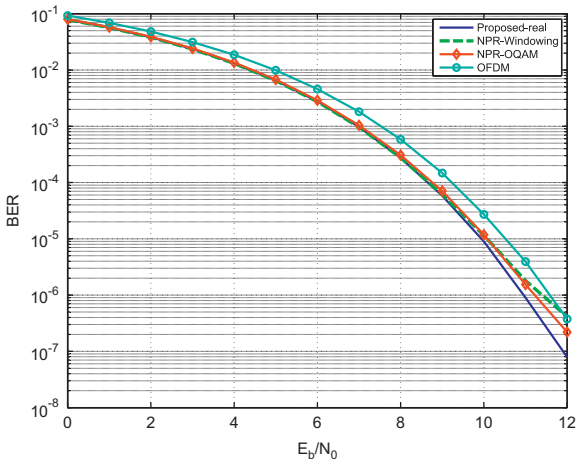

Fig. 9. BER versus E_b/N_0 for different MCM systems with $M=64$ subbands over AWGN channel with carrier frequency offset $\Delta_f = 2\%$.

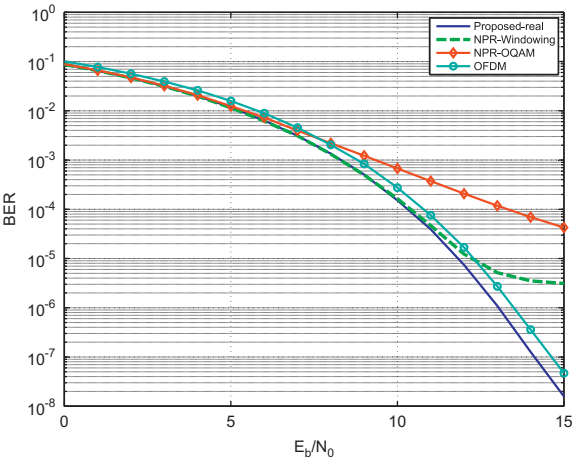

Fig. 10. BER versus E_b/N_0 for different MCM systems with $M=64$ subbands over AWGN channel with carrier frequency offset $\Delta_f = 5\%$.

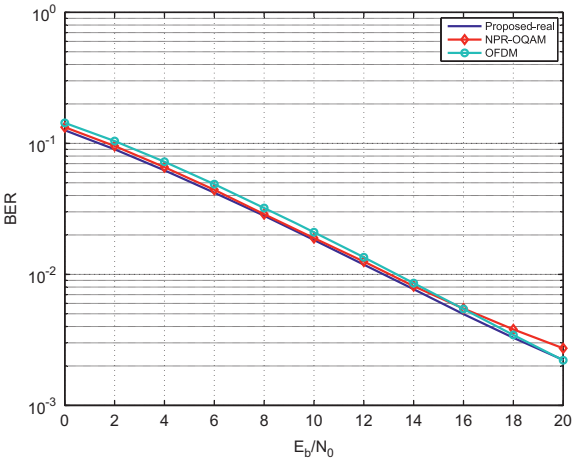

Fig. 11. BER versus E_b/N_0 for different MCM systems with $M=64$ subbands over 5-tap Rayleigh fading channel with carrier frequency offset $\Delta_f = 2\%$.

be vulnerable against CFO, since the subbands are tightly spaced in the transmission band [10,38,39]. By designing sharp filters with much lower sidelobes, we can lessen the effect of CFO. To investigate this effect, we consider a scenario in which the receive FB is not exactly synchronized in frequency with the transmit FB. That is, we introduce a constant frequency offset on all the received tones [38]. This offset, denoted as Δ_f, is measured as percent frequency deviation, relative to the width of a subband, i.e. intercarrier spacing.

Figs. 9 and 10 show the BERs of all previously compared schemes versus SNR over the ideal AWGN channel with $\Delta_f = 2\%$ and $\Delta_f = 5\%$, respectively. Results show that the proposed OPR DFTM FB outperforms OFDM by a margin of more than 0.5 dB. We note that for the particular choice of parameters in Fig. 10, NPR-OQAM is more sensitive to CFO than the other methods under comparison. However, NPR-OQAM can be implemented with different prototype filters whose choice may have an impact on the performance of the FB system in the presence of CFO [39]. Likewise, Figs. 11 and 12 show the BERs versus SNR over the frequency selective channel, where the proposed scheme again offers the best performance.

7. Conclusion

In this paper, a design method for OPR DFTM FBs transceivers was presented. To ensure the PR property of the system, the polyphase matrices of the transmit and the receive FBs were chosen as paraunitary matrices. These matrices were then parameterized, based on factorization methods making use of Givens rotations. Moreover, different methods to reduce the number of parameters were employed and consequently facilitated the optimization process. By minimizing the stop-band energy of the prototype filters with respect to the parameters, prototype filters were designed with good spectral containment such as steeper transition from pass-band to stop-band, lower stop-band energy, and lower sidelobe levels, when compared with OFDM and some recently proposed FBMC

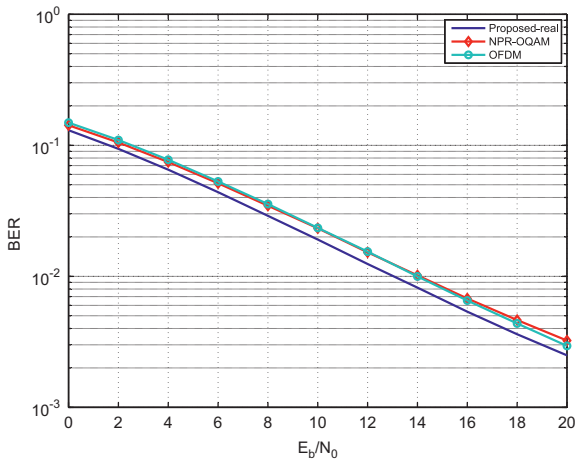

Fig. 12. BER versus E_b/N_0 for different MCM systems with $M=64$ subbands over 5-tap Rayleigh fading channel with carrier frequency offset $\Delta_f = 5\%$.

systems. Numerical experiments show that the proposed scheme offers the lowest BER over AWGN and frequency selective channels. Furthermore, in the presence of NBI or CFO, the proposed FB is more robust against such channel impairments compared to the other MCM systems. These attractive features come at the price of an increase in the computational complexity and processing delay of the system.

Appendix A. Factorization of P(z)

In this Appendix, we show in details how to factorize $\mathbf{P}(z)$ as given by (14). Recall that, $\mathbf{W}$ is the DFT matrix defined as $[\mathbf{W}]_{i,j} = w^{ij}$, $i,j \in \{0,\ldots,M-1\}$ and the block matrices $\mathbf{L}_0$ and $\mathbf{L}_1(z)$, of respective size $D \times M$ and $K \times D$, are defined as follows:

$$\mathbf{L}_0 = [I_M, I_M, \ldots, I_M]^T, \tag{A.1}$$

$$\mathbf{L}_1(z) = [I_K, z^{-1}I_K, \ldots, z^{-(d_K-1)}I_K]. \tag{A.2}$$

Also, diagonal matrix $\mathbf{\Gamma}_f$ is given by

$$\mathbf{\Gamma}_f = \mathrm{diag}(f_0[0], \ldots, f_0[D-1]). \tag{A.3}$$

Let us consider $K \times M$ matrix $\hat{\mathbf{P}}(z)$ as

$$\hat{\mathbf{P}}(z) = \mathbf{L}_1(z)\mathbf{\Gamma}_f\mathbf{L}_0\mathbf{W}^* \tag{A.4}$$

Therefore the (r,i)th entry of $\hat{\mathbf{P}}(z)$ can be written as

$$[\hat{\mathbf{P}}(z)]_{r,i} = \mathbf{L}_{1,r}(z)\mathbf{\Gamma}_f\mathbf{W}_i^*, \tag{A.5}$$

where $1 \times D$ matrix $\mathbf{L}_{1,r}(z)$ is the rth row of $\mathbf{L}_1(z)$ and $D \times 1$ matrix $\mathbf{W}_i$ is the product of $\mathbf{L}_0$ and ith column of $\mathbf{W}^*$.

$$\mathbf{L}_{1,r}(z) = [\ldots, 0, 1, 0, \ldots, 0, z^{-1}, 0, \ldots, 0, z^{-(dK-1)}, 0, \ldots] \tag{A.6}$$

Note that non-zero elements of $\mathbf{L}_{1,r}(z)$ are situated at $(nK + r)$ th columns, where $n \in \{0,\ldots,d_K-1\}$. Consequently, we can further simplify the product of $\mathbf{L}_{1,r}(z)\mathbf{\Gamma}_f$ and write

$$\mathbf{L}_{1,r}(z)\mathbf{\Gamma}_f = [\ldots, 0, f_0[r], 0, \ldots, 0, f_0[K+r]z^{-1}, 0, \ldots, 0, f_0[(dK-1)K+r]z^{-(dK-1)}, 0, \ldots] \tag{A.7}$$

Moreover, considering the fact that $w^{M+c} = w^c$, $D \times 1$ matrix $\mathbf{W}_i$ can be simplified as

$$\mathbf{W}_i = \begin{bmatrix} I_M \\ I_M \\ \vdots \\ I_M \end{bmatrix} \begin{bmatrix} w^{-0i} \\ w^{-1i} \\ w^{-2i} \\ \vdots \\ w^{-(M-1)i} \end{bmatrix} = \begin{bmatrix} w^{-0i} \\ \vdots \\ w^{-(M-1)i} \\ w^{-0i} \\ \vdots \\ w^{-(M-1)i} \\ \vdots \\ w^{-0i} \\ \vdots \\ w^{-(M-1)i} \end{bmatrix} = \begin{bmatrix} w^{-0i} \\ \vdots \\ w^{-(M-1)i} \\ w^{-Mi} \\ \vdots \\ w^{-(2M-1)i} \\ \vdots \\ w^{-(D-M)i} \\ \vdots \\ w^{-(D-1)i} \end{bmatrix} \tag{A.8}$$

Finally, by substituting (A.(7) and A.8) in (A.5) we can write

$$[\hat{\mathbf{P}}(z)]_{r,i} = \sum_{n=0}^{d_K-1} f_0[nK+r]w^{-i(nK+r)}z^{-n}, \tag{A.9}$$

which is in full accordance with (7). Thus, it can be stated that $\hat{\mathbf{P}}(z) = \mathbf{P}(z)$ and Eq. (14) is verified.

$$\mathbf{P}(z) = \mathbf{L}_1(z)\mathbf{\Gamma}_f\mathbf{L}_0\mathbf{W}^*. \tag{A.10}$$

References

[1] R. Van Nee, R. Prasad, OFDM for Wireless Multimedia Communications, Norwood, MA, USA, 2000.

[2] A.J. Coulson, Bit error rate performance of OFDM in narrowband interference with excision filtering, IEEE Transactions on Wireless Communications 5 (2006) 2484–2492.

[3] P. Moose, A technique for orthogonal frequency division multiplexing frequency offset correction, IEEE Transactions on Communications 42 (1994) 2908–2914.

[4] T. Pollet, M. Van Bladel, M. Moeneclaey, BER sensitivity of OFDM systems to carrier frequency offset and Wiener phase noise, IEEE Transactions on Communications 43 (1995) 191–193.

[5] P.P. Vaidyanathan, Multirate Systems and Filter Banks, Prentice-Hall, Upper Saddle River, NJ, USA, 1993.

[6] B. Farhang-Boroujeny, OFDM versus filter bank multicarrier, IEEE Signal Processing Magazine 28 (2011) 92–112.

[7] G. Cherubini, E. Eleftheriou, S. Olcer, Filtered multitone modulation for very high-speed digital subscriber lines, IEEE Journal on Selected Areas in Communications 20 (2002) 1016–1028.

[8] C. Siclet, P. Siohan, D. Pinchon, Perfect reconstruction conditions and design of oversampled DFT-modulated transmultiplexers, EURASIP Journal on Advances in Signal Processing 2006 (2006), 14 (Article ID 15756).

[9] F. Duplessis-Beaulieu, B. Champagne, Design of prototype filters for perfect reconstruction DFT filter bank transceivers, Signal Processing 89 (2009) 87–98.

[10] S. Rahimi, B. Champagne, On the robustness of oversampled filter bank multi carrier systems against frequency offset, in: Proceedings of the ISWCS, August 2012, Paris, France.

[11] M. Bellanger, Specification and design of a prototype filter for filter bank based multicarrier transmission, in: Proceedings of the ICASSP, May 2001, Salt Lake City, UT, USA, pp. 2417–2420.

[12] P. Siohan, C. Siclet, N. Lacaille, Analysis and design of OFDM/OQAM systems based on filterbank theory, IEEE Transactions on Signal Processing 50 (2002) 1170–1183.

[13] A. Viholainen, T. Ihalainen, T. Stitz, M. Renfors, M. Bellanger, Prototype filter design for filter bank based multicarrier transmission, in: Proceedings of the EUSIPCO, Glasgow, Scotland, August 2009, pp. 1359–1363.

[14] M. Bellanger, et al., FBMC Physical Layer: A Primer, PHYDYAS, January 2010.

[15] S.-M. Phoong, Y. Chang, C.-Y. Chen, DFT-modulated filterbank transceivers for multipath fading channels, IEEE Transactions on Signal Processing 53 (2005) 182–192.

[16] S. Rahimi, B. Champagne, Perfect reconstruction DFT modulated oversampled filter bank transceivers, in: Proceedings of the EUSIPCO, Barcelona, Spain, Auguat 2011, pp. 1588–1592.
[17] L. Lin, B. Farhang-Boroujeny, Cosine-modulated multitone for very-high-speed digital subscriber lines, EURASIP Journal on Applied Signal Processing (2006) 16 (Article ID 19329).
[18] P. Martin-Martin, R. Bregovic, A. Martin-Marcos, F. Cruz-Roldan, T. Saramaki, A generalized window approach for designing trans-multiplexers, IEEE Transactions on Circuits and Systems 55 (2008) 2696–2706.
[19] F. Mintzer, On half-band, third-band, and Nth-band FIR filters and their design, IEEE Transactions Acoustics, Speech and Signal Processing 30 (1982) 734–738.
[20] N. Benvenuto, S. Tomasin, L. Tomba, Equalization methods in OFDM and FMT systems for broadband wireless communications, IEEE Transactions on Communications 50 (2002) 1413–1418.
[21] P. Vaidyanathan, Theory and design of M-channel maximally decimated quadrature mirror filters with arbitrary M, having the perfect-reconstruction property, IEEE Transactions on Acoustics, Speech and Signal Processing 35 (1987) 476–492.
[22] X. Gao, T. Nguyen, G. Strang, On factorization of M-channel paraunitary filterbanks, IEEE Transactions on Signal Processing 49 (2001) 1433–1446.
[23] L. Gan, K.-K. Ma, On simplified order-one factorizations of paraunitary filterbanks, IEEE Transactions on Signal Processing 52 (2004) 674–686.
[24] D. Pinchon, P. Siohan, Oversampled paraunitary DFT filter banks: a general construction algorithm and some specific solutions, IEEE Transactions on Signal Processing 59 (2011) 3058–3070.
[25] Y.-J. Chen, S. Oraintara, K. Amaratunga, Dyadic-based factorizations for regular paraunitary filterbanks and M-band orthogonal wavelets with structural vanishing moments, IEEE Transactions on Signal Processing 53 (2005) 193–207.
[26] S. Weiss, R.W. Stewart, Fast implementation of oversampled modulated filter banks, Electronics Letters 36 (2000) 1502–1503.
[27] G. Hardy, E. Wright, J. Silverman, An Introduction to the Theory of Numbers, Oxford University Press, New York, USA, 2008.
[28] Z. Cvetkovic, M. Vetterli, Tight Weyl-Heisenberg frames in $l^2(z)$, IEEE Transactions on Signal Processing 46 (1998) 1256–1259.
[29] R. Raffenetti, K.C. Ruedenberg, Parametrization of an orthogonal matrix in terms of generalized Eulerian angles, Journal of Quantum Chemistry III S (1969) 625–634.
[30] G. Golub, C. Van Loan, Matrix Computations, Johns Hopkins University Press, Baltimore, MD, 1996.
[31] J. Nocedal, S.J. Wright, Numerical Optimization, Springer, Berlin, 2000.
[32] L. Vangelista, N. Benvenuto, S. Tomasin, C. Nokes, J. Stott, A. Filippi, M. Vlot, V. Mignone, A. Morello, Key technologies for next-generation terrestrial digital television standard DVB-T2, IEEE Communications Magazine 47 (2009) 146–153.
[33] Z. Cvetkovic, M. Vetterli, Oversampled filter banks, IEEE Transactions on Signal Processing 46 (1998) 1245–1255.
[34] Z. Cvetkovic, Modulating waveforms for OFDM, in: Proceedings of the ICASSP, vol. 5, Washington, DC, USA, (1999) pp. 2463–2466.
[35] A. Tonello, F. Pecile, Efficient architectures for multiuser FMT systems and application to power line communications, IEEE Transactions on Communications 57 (2009) 1275–1279.
[36] D. Umehara, H. Nishiyori, Y. Morihiro, Performance evaluation of CMFB transmultiplexer for broadband power line communications under narrowband interference, in: Proceedings of the International Symposium on Power Line Communications and its Applications, Orlando, USA, March 2006, pp. 50–55.
[37] F. Duplessis-Beaulieu, B. Champagne, One-tap equalizer for perfect reconstruction DFT filter bank transceivers, in: Proceedings of the International Symposium on Signals, Systems and Electronics, Montreal, Canada, August 2007, pp. 391–394.
[38] T. Fusco, A. Petrella, M. Tanda, Sensitivity of multi-user filter-bank multicarrier systems to synchronization errors, in: Proceedings of the ISCCSP, St. Julians, Malta, March 2008, pp. 393–398.
[39] H. Saeedi-Sourck, Y. Wu, J.W. Bergmans, S. Sadri, B. Farhang-Boroujeny, Sensitivity analysis of offset QAM multicarrier systems to residual carrier frequency and timing offsets, Signal Processing 91 (2011) 1604–1612.